Multi-Parameter Sensors Based on Optical Reflective Coupler Probe

Yufang Chen, Hongdan Wan, Zhongwei Liang, Yao Lu, and Fangren Hu

***Abstract*— We propose and demonst rate multi-parameter sensors based on optical reflective coupler probe (ORCP), for detection of liquid level, temperature, and refractive index (RI). Single-mode fiber ORCP (S-ORCP), few-mode fiber ORCP (F-ORCP) and multi-mode fiber ORCP (M-ORCP) are fabricated by adiabatically tapering and weak fusion technology. The highest liquid level sensitivity is 363.64 nm/mm, achieved by the M-ORCP, with detection limit of as low as 0.06 μm. In addition, multi-parameter measurement of liquid level, temperature and RI can be achieved by the M-ORCP, with temperature and RI sensitivities of −0.327 nm/°C and 7859.27 nm/RIU, respectively. With the merits of high sensitivity, stability, and compact half-coupler probe structure, the proposed ORCP sensors of ∼ cm length can measure the liquid level range of ∼3 mm, which have broad application prospects in the fields of fuel storage and chemical liquid level measurement, especially for chemical reagents, biological tissue liquids and flammable and explosive liquids.**

***Index Terms*—Liquid level sensor, multi-parameter, optical reflective coupler probe, low detection limit.**

I. Introduction

LIQUID level sensing is of particular significance and widely used in industrial and applications such as fuel storage, chemical synthesis, and biological analysis. Different liquid level sensors have been reported based on mechanical, electrical, and optical methods [1], [2]. Due to the inherent advantages of miniature size, electromagnetic immunity, resistance to corrosion, and remote sensing capability, the optical fiber liquid level sensors (OFLLSs) are extensively employed.

So far, different types of OFLLSs have been proposed, including interferometric structures [3], [4], [5], [6], [7], fiber gratings [8], [9], [10] and special microstructures [11], [12]. Wavelength or intensity modulation are the two main demodulation parameters for liquid level measurement [3], [4], [5], [6], [7], [8], [9], [10], [11], [12], [13]. Liu et al. demonstrated a high refractive index (RI) OFLLS based on coreless multi-mode fiber with a linear response of −0.461 dB/mm [3]. Liu et al. proposed an OFLLS based on a fiber ball-thin fiber-core offset structure with a sensitivity of −0.121 nm/mm [4]. Zhang et al. implemented an OFLLS based on reflective long-period fiber grating with a sensitivity of 0.772 dB/mm [9]. Sun et al. proposed an OFLLS based on a microfiber probe with a sensitivity of 367.644 nm/mm [13]. The intensity-modulated sensor has good stability and simplified constructions. However, the main challenge is to enhance sensitivity and reduce crosstalk.

Among the physical variables which affect the OFLLSs, temperature is the most relevant in this application. Dong et al. proposed an OFLLS based on coreless-D-shape-coreless fiber structure with a sensitivity of 213.8 pm/mm and a temperature crosstalk of −0.128 mm/°C [11]. Kang et al. proposed a novel in-fiber modal interferometer for liquid level sensing based on the cascaded quasi-microfiber and double-cladding fiber with a response of −0.972 dB/mm and a temperature sensitivity of 0.164 nm/°C [6]. The composite schemes with embedded FBGs are utilized to eliminate the inaccuracy of the measured liquid level caused by temperature crosstalk [10], [14]. Camilo et al. proposed an OFLLS based on a FBG embedded into an epoxy resin diaphragm with a liquid level sensitivity of 2.8 pm/mm and a lower temperature crosstalk of 1.04 mm/°C [10]. In addition, the temperature-insensitive characteristics of photonic crystal fiber are utilized to solve the temperature crosstalk with a liquid level sensitivity of 0.585 nm/mm [12]. For most of OFLLSs, especially for application in dangerous chemical liquid with high risk of explosion or combustion, the sensitivity is still insufficient for liquid level measurement within a small measurement range of 3 mm. It is necessary to pursue higher sensitivity and lower temperature crosstalk [15].

The above reports have important applications in detecting relevant physical parameters, but few reports execute the multi-parameter detection of liquid level, temperature, and RI in liquid. Recently, high sensitivity detection for temperature, RI, other biomolecular and virus molecular is achieved by interferometers based on optical microfiber couplers (OMCs) [16], [17]. Theoretical analysis in [18], [19] demonstrated that the temperature and RI sensitivity of the OMCs could be infinity near the dispersion turning point. However, as far as we know, there is no report of using OMCs for multi-parameter detection of liquid level and other parameters, especially with high sensitivity.

Manuscript received 29 May 2022; revised 6 August 2022; accepted 17 August 2022. Date of publication 22 August 2022; date of current version 31 August 2022. This work was supported in part by the National Natural Science Foundation of China under Grants 12174199 and 11704199, in part by the China Postdoctoral Science Foundation under Grant 2021M701765, in part by the General Program of Natural Science Foundation of Jiangsu Province under Grant BK20221330, in part by the Jiangsu University 'Blue Project' Funding, in part by the Postgraduate Research and Practice Innovation Program of Jiangsu Province under Grants KYCX22_0988, KYCX22_0911, and KYCX22_0912, and in part by the STITP of NUPT under Grant SZDG2021013. *(Corresponding author: Hongdan Wan.)*

Yufang Chen, Hongdan Wan, Zhongwei Liang, and Yao Lu are with the Advanced Photonic Technology Lab, Nanjing University of Posts and Telecommunications, Nanjing 210023, China (e-mail: 1361977250@qq.com; hdwan@njupt.edu.cn; 384191084@qq.com; 1469251900@qq.com).

Fangren Hu is with the College of Electronic and Optical Engineering and College of Flexible Electronics (future technology), Nanjing University of Posts and Telecommunications, Nanjing 210023, China (e-mail: hufr@njupt).

Digital Object Identifier 10.1109/JPHOT.2022.3200712

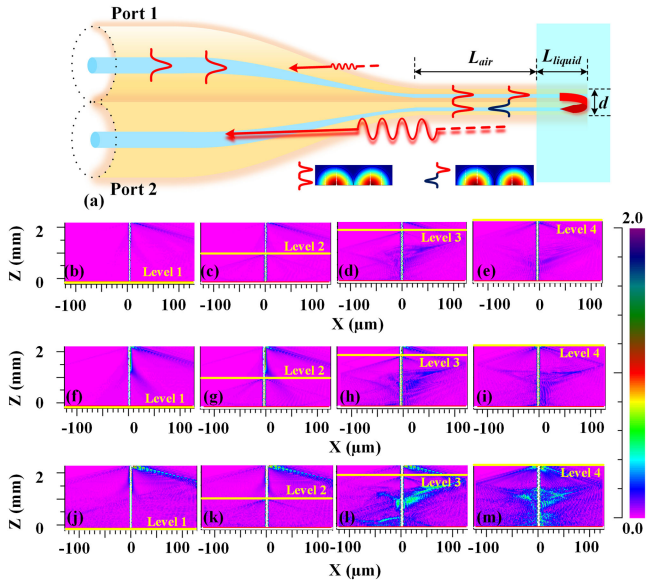

Fig. 1. Simulation analysis: (a) Schematic diagram of the ORCP; Simulated amplitude distribution within coupling region along the: (b)–(e) S-ORCP; (f)–(i) F-ORCP; (j)–(m) M-ORCP. The liquid levels (yellow lines) from level 1 to level 4 are 0 mm, 1.115 mm, 1.965 mm, and 2.29 mm, respectively.

In this paper, we propose and demonstrate multi-parameter sensors based on optical reflective coupler probe (ORCP) for detection of liquid level, temperature, and RI. The OFLLSs based on three kinds of ORCPs are fabricated by adiabatically tapering and weak fusion technology, including single-mode fiber ORCP (S-ORCP), the few-mode fiber ORCP (F-ORCP) and the multi-mode fiber ORCP (M-ORCP). The liquid level sensitivities of S-ORCP and F-ORCP are 43.71 nm/mm and 65.14 nm/mm. The highest liquid level sensitivity is achieved by the M-ORCP with 363.64 nm/mm and the detection limit is as low as 0.06 μm. In addition, the temperature and RI can also be detected by the M-ORCP, with sensitivities of -0.327 nm/°C and 7859.27 nm/RIU. The proposed ORCP sensors of $\sim$ cm length can measure the liquid level range of $\sim$3 mm due to the merits of high sensitivity, stability, and compact half-coupler probe structure, which has broad application prospects in the fields of fuel storage and chemical liquid level measurement, especially for chemical reagents, biological tissue liquids and flammable and explosive liquids.

II. Theoretical Analysis

The proposed S-ORCP, F-ORCP and M-ORCP were fabricated with two single-mode fibers (SMF, core/cladding diameter = 8.2/125 μm, NA = 0.14), or two few-mode fibers (FMF, core/cladding diameter = 19/125 μm, NA = 0.15), or two multimode fibers (MMF, core/cladding diameter = 50/125 μm, NA = 0.2) to form OMC by weak fusion technology [20]. Then the waist region of the fabricated OMC is cut vertically to form a Fresnel reflection end face. Fig. 1(a) is the schematic diagram of the proposed ORCP. L_{air} and L_{liquid} are the coupling length in air and liquid. d is the waist diameter of the ORCP. According to the supermodes theory, the two parallel tapered fibers are regard as a new waveguide. When light injects into port 1 and reaches the coupling region, the even- and odd-supermodes are excited and interfere with each other. Due to the effective RI difference between the two supermodes, optical interference effect is generated with an optical phase difference (OPD) decided by liquid level. The light is then reflected at the end face of the ORCP owing to the Fresnel reflection. Most of the light is reflected into port 2 and a small part of light is reflected into port 1. Thus, the coupling length and the OPD are doubled. The reflection spectrum of the ORCP can be measured at port 2. Fig. 1(b)–(e), (f)–(i) and (j)–(m) are the simulation results of amplitude distribution along the S-ORCP, F-ORCP and M-ORCP by using beam propagation method (BPM), the yellow lines represent different liquid levels (level 1 to level 4). The surrounding RI and operation wavelength are 1.0 and 1550 nm. d is $\sim$2.5 μm. The coupling length ($L_{air} + L_{liquid}$) is $\sim$2.29 mm. The interference intensity distribution of the light field in the coupling region takes on a typical 'snake' shape both in air and liquid. As the liquid level increased from 0 mm to 2.29 mm, the immersed part has the enhanced evanescent wave. The spectra of the ORCPs will change accordingly, due to mode interference is varied by different OPD. As for FMF and MMF, higher-order modes have stronger field in the cladding region [21]. From the simulation and comparison, it can be seen that as compared with the S-ORCP, more modal power in the cladding of F-ORCP and M-ORCP are converted into evanescent field. Thus, the F-ORCP and M-ORCP have larger evanescent field leakage, indicating they can achieve higher sensitivity.

According to the supermode theory, the output power R_2 at port 2 are expressed by the following equations [22]:

$$R_2 = \frac{1}{2}A\left[1-\cos^2\theta\cos^2\left(\frac{1}{2}\varphi_x\right)+\sin^2\theta\cos^2\left(\frac{1}{2}\varphi_y\right)\right] \quad (1)$$

where θ is the input light and the angle between the polarized plane and the horizontal axis. $A = (n_1-n_0)^2/(n_1+n_0)^2$. n_1 and n_0 are the refractive index of silica and air, respectively. The total OPD ($\varphi_{i[i\,=\,x,y]}$) in the sensor can be defined as:

$$\begin{aligned}\varphi_i &= \frac{\pi}{\lambda}\left(n_{eff}^{even}-n_{eff}^{odd}\right)\cdot 2L \\ &= \frac{2\pi}{\lambda}\left(\Delta n_{air}\cdot L_{air}+\Delta n_{liquid}\cdot L_{liquid}\right)\end{aligned} \quad (2)$$

where λ is the operating wavelength, Δn_{air} and Δn_{liquid} are the effective RI differences ($n_{eff}^{even} - n_{eff}^{odd}$) between the two interference supermodes in air and liquid, respectively. $\Delta n_{air} = (n_{eff}^{even} - n_{eff}^{odd})_{air}$, $\Delta n_{liquid} = (n_{eff}^{even} - n_{eff}^{odd})_{liquid}$, L is the total length of the ORCP ($L = L_{air} + L_{liquid}$). When the φ is satisfied $\varphi = (2N+1)\pi$, $N = 0,1,2,3\ldots$, N is an integer, the destructive interference condition is satisfied. The dip wavelength λ_N can be calculated as:

$$\begin{aligned}\lambda_N &= \frac{2(\Delta n_{air}\cdot L_{air}+\Delta n_{liquid}\cdot L_{liquid})}{2N+1} \\ &= \frac{2L_{liquid}(\Delta n_{air}-\Delta n_{liquid})+2L\Delta n_{air}}{2N+1}\end{aligned} \quad (3)$$

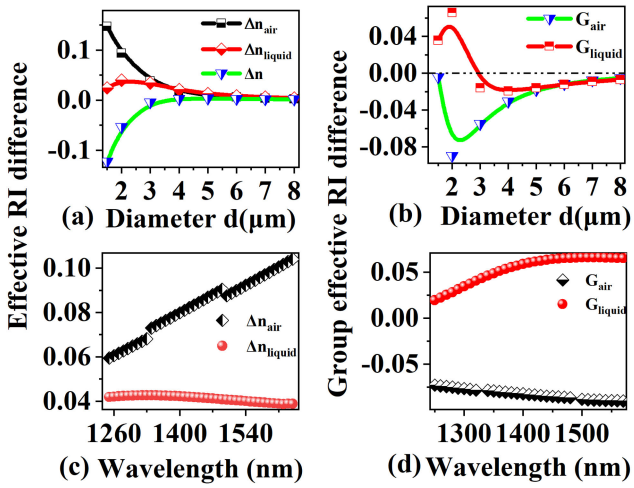

Fig. 2. The simulation and comparison results between the two supermodes in air and liquid of S-ORCP. The relationship between: (a) Effective RI difference; (b) Group effective RI difference and diameter; The relationship between: (c) Effective RI difference; (d) Group effective RI difference and wavelength.

The free spectral range (FSR) of the probe is expressed as:

$$FSR = \frac{\lambda^2}{\Delta n_{air} L_{air} + \Delta n_{liquid} L_{liquid}} \tag{4}$$

The response sensitivity of liquid level at resonant dip λ_N can be given as:

$$S = \frac{\partial \lambda_N}{\partial L_{\text{liquid}}} = \frac{\lambda_N (\Delta n_{liquid} - \Delta n_{air})}{L_{\text{liquid}} G_{liquid} + L_{air} G_{air}} \tag{5}$$

$$G_{liquid} = \Delta n_{liquid} - \lambda_N \frac{\partial \Delta n_{liquid}}{\partial \lambda_N} \tag{6}$$

$$G_{air} = \Delta n_{air} - \lambda_N \frac{\partial \Delta n_{air}}{\partial \lambda_N} \tag{7}$$

where G_{liquid} and G_{air} are the group effective RI difference between the two interference supermodes in liquid and air, respectively.

Fig. 2(a) is the calculated Δn_{air} and Δn_{liquid} in the ambient RI of 1.0000 and 1.3333 as a function of the S-ORCP's diameter. It can be seen the Δn_{air} is larger than the Δn_{liquid}, while the $|\Delta n|$ ($\Delta n = \Delta n_{liquid}$-$\Delta n_{air}$) is gradually reduced. From (6) and (7), the group effective RI differences of the S-ORCP with different waist diameters in the liquid and air are shown in Fig. 2(b). As for G_{liquid}, there is a turning point from positive to negative while the G_{air} is always negative and is smaller than the G_{liquid}. From (5) and Fig. 2, the liquid level sensitivity is affected by d and L. The change in liquid level can change L_{liquid} and L_{air} to influence the sensitivity. Fig. 2(c) and (d) are the relationship between effective RI difference or group effective RI difference and wavelength. As wavelength is increased from 1250 nm to 1650 nm, the calculated effective RI difference and group effective RI difference in air and liquid are different, which indicates the modal intensity distribution of supermodes will change with wavelength. The optical power in core and cladding of S-ORCP, F-ORCP and M-ORCP at different wavelength are also calculated. The optical power distribution is various at different wavelength. Thus, the mode and power distribution are wavelength dependent for the S-ORCP, F-ORCP and M-ORCP.

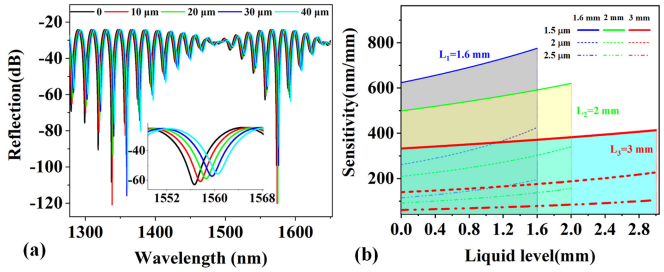

Fig. 3. Simulated results of the S-ORCP: (a) The reflection spectra with different liquid levels near wavelength of 1550 nm; (b) The relationship between the liquid level sensitivities and the liquid level at different diameters and coupling lengths.

Fig. 3(a) is the simulated reflection spectra of the S-ORCP near wavelength of 1550 nm with different L_{liquid} (L_{liquid} = 0 μm, 10 μm, 20 μm, 30 μm, 40 μm). d is 2.5 μm and L is fixed at 3 mm. The RI of the liquid is 1.3333. The reflection wavelength red-shifts as the L_{liquid} is increased from 0 μm to 40 μm. Fig. 3(b) shows the relationship between the liquid level sensitivities and the liquid level with different ds (three line-types: 1.5 μm, 2 μm, 2.5 μm), and Ls (three color areas: 1.6 mm, 2 mm, 3 mm). For the fixed liquid levels, d decreases and the sensitivity becomes larger. For the same d, L decreases and the sensitivity becomes larger. The smaller the L and d, the larger the liquid level sensitivity. However, the smaller L limits the measurement range. There is a turnoff between the sensitivity and measurement range. For the S-ORCP with L = 3 mm, the simulated sensitivities with d = 1.5 μm, 2 μm and 2.5 μm are 332.77 nm/mm, 139.57 nm/mm, and 61.30 nm/mm, respectively.

III. Sensor Fabrication and Experimental Setup

In order to fabricate the ORCPs, it is necessary to obtain the OMCs firstly. Two fibers (SMFs, FMFs or MMFs) are aligned with each other before they are fused together using the flame modification method. During the fabrication process, the hydrogen gas flow, stretching speed and length, which determine the performance of the OMCs are controlled and optimized. Then, the proposed ORCPs are fabricated with a gem knife, by snapping the waist region of the OMCs to form the Fresnel reflection end faces. A broadband source (BBS, with wavelength ranging from 1250 nm to 1650 nm) is connected to the port 1 of the ORCP. The reflection spectra of the ORCP are recorded by an optical spectrum analyzer (OSA, AQ6370D, with bandwidth resolution of 0.02 nm, from 900 nm–1700 nm) real time through port 2. Fig. 4(a) and (b) show the microscopic images of the S-ORCP, L is ~3 mm. Fig. 4(c) shows the cross-section image of the S-ORCP, d is ~2.5 μm. Fig. 4(d) is comparison of the measured reflection spectra of the S-ORCP in air and liquid, respectively. When the S-ORCP is immersed in liquid from air gradually, the loss increases from 16.168 dB to 32.347 dB and the spectra shifts to longer wavelength, which is consistent with the results in Fig. 3.

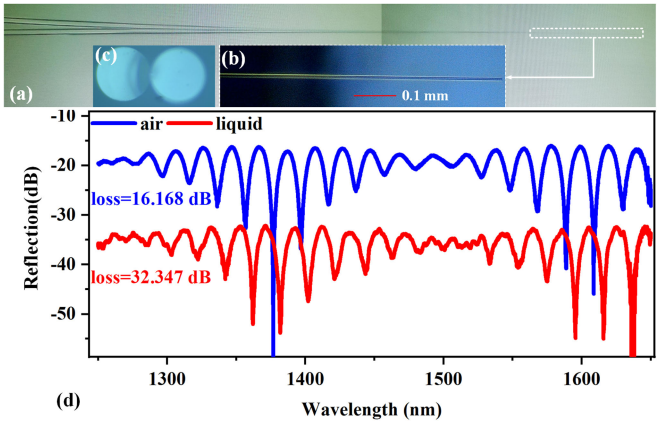

Fig. 4. Microscopic images and the measured results of the S-ORCP: (a) and (b) At the coupling region; (c) At the fiber cross-section; (d) The measured reflection spectra in air and liquid, respectively.

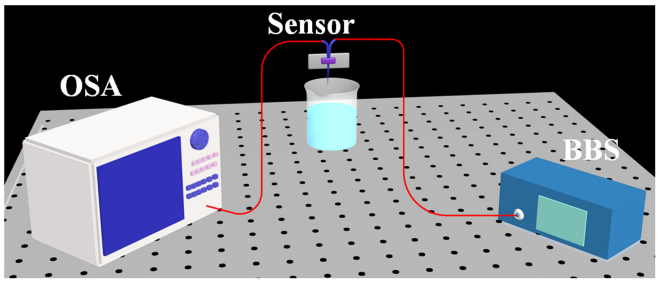

Fig. 5. Schematic diagram of the proposed OFLLS.

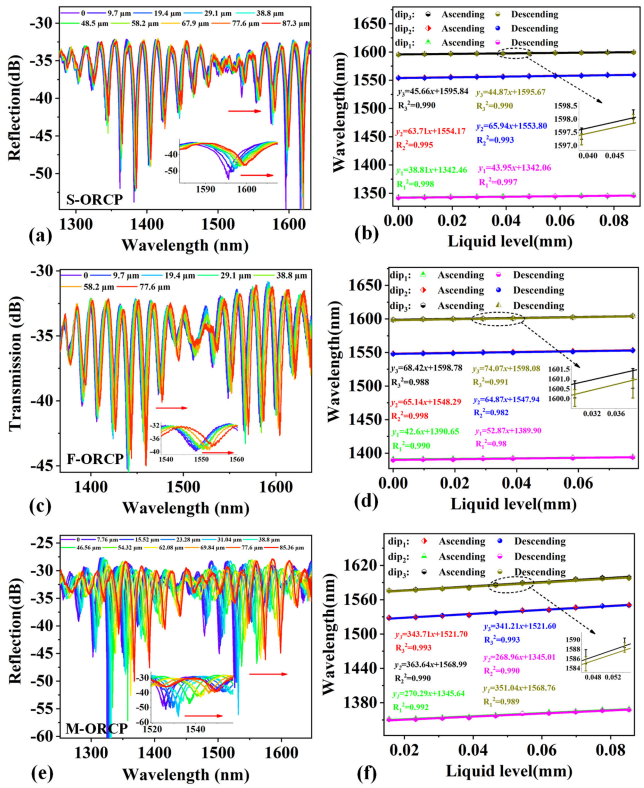

Fig. 6. Measured liquid level response of the OFLLSs based on: (a) and (b) S-ORCP; (c) and (d) F-ORCP; (e) and (f) M-ORCP.

Fig. 5 shows the schematic diagram of the proposed OFLLS based on the ORCPs. The system consists of a BBS, an ORCP, a beaker, and an OSA. The packaged ORCP is dipping vertically into the beaker and contacting the lower end of the sensor region with the liquid level. For the ORCPs with appropriate d ($\geq$2.5 μm), the buoyancy variation can hardly affect the spectra due to the high Young's modulus of silica fibers and the surface tension between liquid and fiber is small, which can be neglected [15]. The liquid level variation was characterized by repeatedly adding or remove liquid with a pipette of 20 μL that is equivalent to a calculated minimum level change of 3.88 μm (The diameter of the beaker is 80.97 mm).

IV. Experiment And Results

Fig. 6 shows the liquid level response of S-ORCP, F-ORCP and M-ORCP. Fig. 6(a) is the measured reflection spectra of S-ORCP with different liquid levels. It is clear that the reflection wavelengths shifted as the liquid level is increased from 0 mm to 87.3 μm with a step of 9.7 μm. The inset is the wavelength shift measured near 1550 nm. As the liquid level increases, the spectral drift is more obvious at longer wavelength. However, the longer the wavelength, the greater the absorption loss of water. There should be a compromise between the sensitivity and the loss. Fig. 6(b) shows the repeatability and the fitting curves of the wavelength drift versus the liquid level at the wavelength of 1350 nm, 1550 nm, and 1600 nm. When the liquid level is increased, the wavelength red-shifts with sensitivities of 38.81 nm/mm, 43.71 nm/mm, and 45.66 nm/mm, respectively. The linearity (R^2) is measured to be about 0.990. When the liquid level decreases, the wavelength blue-shifts accordingly and with sensitivities of 43.95 nm/mm, 43.94 nm/mm, and 44.87 nm/mm. Repeatedly testing the drift of the S-ORCPs at different liquid levels to research the repeatability of the proposed OFLLS. In Fig. 6(b), the inset is the detail measurement error around 1600 nm. The maximum non-repeatability of the wavelength drift is $\sim\pm$0.25 nm, due to the evaporation of water molecules and a small amount of water molecules carried by the S-ORCP. Hence, the proposed S-ORCP possesses good reversibility and repeatability in measuring liquid level.

In order to further improve the liquid level sensitivity of the proposed OFLLS, FMF and MMF are used to fabricate F-ORCP and M-ORCP ($d = 2.5$ μm and $L = 3$ mm). Fig. 6(c) and (d) are the liquid level response of the OFLLS based on F-ORCP. When the liquid level is increased, the wavelength red-shifts with sensitivities of 42.6 nm/mm, 65.14 nm/mm, and 68.42 nm/mm, respectively. As the liquid level decreased, the wavelength blue-shifts accordingly and with sensitivities of 52.87 nm/mm, 64.87 nm/mm, and 74.07 nm/mm. The R^2 is $\sim$0.990 and the maximum non-repeatability of the wavelength drift is $\sim\pm$0.21 nm. For the OFLLS based on M-ORCP, the maximum measured sensitivity is 363.64 nm/mm around 1550 nm in Fig. 6(e). The detection limit for the M-ORCP is as low as 0.06 μm. In Fig. 6(f), the measured maximum non-repeatability of the wavelength drift is $\sim\pm$0.45 nm. The sensitivities for

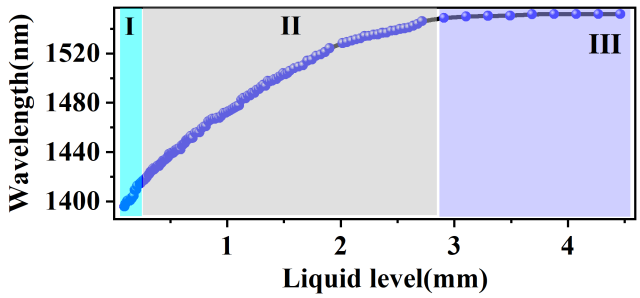

Fig. 7. The wavelength shifts of M-ORCP around 1400 nm at each liquid level.

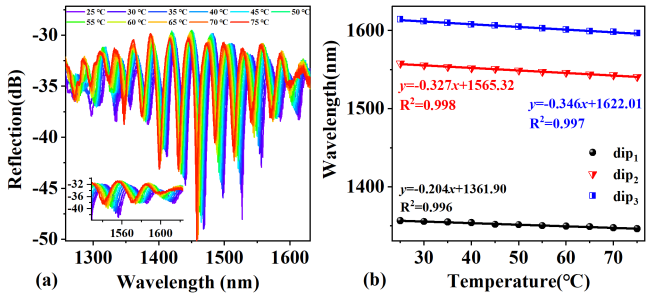

Fig. 8. Measured temperature characteristics of the M-ORCP packaged in water-filled capillary: (a) The reflection spectra with increased temperature; (b) The corresponding relationship between wavelength and temperature.

F-ORCP and M-ORCP are higher than the S-ORCP, which is consistent with the simulation results in Fig. 1.

With further increase of liquid level, the spectral wavelength shift tends to be stable. Fig. 7 shows the wavelength shift of M-ORCP around 1400 nm at each liquid level. The curve of liquid level response exhibits nonlinear in the whole measurement range from 0 to 4.5 mm, including linear (I), transition (II) and saturation (III) zones. Zone 1 has a maximum sensitivity of 363.64 nm/mm. As the liquid level increases to ∼3 mm (II), the wavelength shift decreases as well as sensitivity. In addition, when the liquid level is ∼3 mm, the wavelength shift tends to be stable.

The temperature characteristic of the proposed M-ORCP is also demonstrated. The M-ORCP is completely encapsulated in a capillary filled with water (RI = 1.3333) and is placed in a temperature controller with a resolution of 0.1 °C. Fig. 8(a) and (b) are the temperature response of the M-ORCP in liquid. When the ambient temperature was raised from 25 °C to 75 °C with a temperature interval of 5 °C, the wavelength dip blue-shifts and the sensitivities are −0.204 nm/°C, −0.327 nm/°C and −0.346 nm/°C around 1350 nm, 1550 nm, and 1600 nm, respectively. The reflection spectral responses of the liquid level and temperature in liquid are different, indicating the proposed sensor can be used for measurement of liquid and temperature [23]. The RI of liquid is inversely proportional to temperature [24]. The higher the temperature is, the more active the molecules are, the smaller the molecular density is, and the smaller the RI is, causing a blue shift.

The response of the M-ORCP in different RI solutions were tested by tracing the shifting of peaks in reflection spectra. The

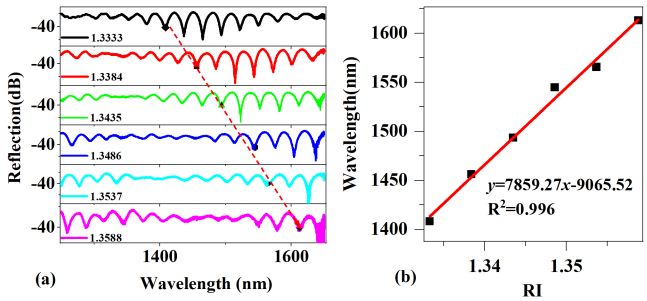

Fig. 9. Reflection spectra versus the RI vibration: (a) The reflection spectra at different RI; (b) The fitting curves of wavelength drift versus RI.

prepared solutions are five kinds of NaCl solutions with different concentrations. The RI of the solution is measured for 3 times by abbe refractometer and averaged, ranging from 1.3333 to 1.3588. As demonstrated in Fig. 9(a), the peaks red-shift dramatically with increase of the RI. Fig. 9(b) shows the measured wavelength as a function of the different RIs of the NaCl solutions. The RI sensitivity is 7859.27 nm/RIU, with R^2 of 0.996.

The interference dips formed between even- and odd- supermodes exhibits different characteristics. Due to the proposed ORCPs have different spectral response of liquid level and temperature, the sensor can be used for detection of liquid level and temperature. Selecting two interference dips as the observation spots and the multi-parameter measurement of liquid level and temperature can be realized by the sensitive matrix. The relationship between the wavelength drift and liquid level and temperature is expressed as [12]:

$$\begin{bmatrix} \Delta\lambda_1 \\ \Delta\lambda_2 \end{bmatrix} = \begin{bmatrix} K_1^L & K_1^T \\ K_2^L & K_2^T \end{bmatrix} \begin{bmatrix} \Delta L \\ \Delta T \end{bmatrix} \tag{8}$$

where $\Delta\lambda_1$ and $\Delta\lambda_2$ represent wavelength drifts around 1550 nm (dip 1) and 1600 nm (dip 2), respectively. K_1^L and K_1^T are the liquid level and temperature sensitivity of dip 1. K_2^L and K_2^T are the liquid level and temperature sensitivity of dip 2. ΔL and ΔT represent the variations of liquid level and temperature, respectively. According to the change principle of the inverse matrix, the matrix (8) can be written as:

$$\begin{bmatrix} \Delta L \\ \Delta T \end{bmatrix} = \frac{1}{K_2^T K_1^L - K_2^L K_1^T} \begin{bmatrix} K_2^T & -K_1^T \\ -K_2^L & K_1^L \end{bmatrix} \begin{bmatrix} \Delta\lambda_1 \\ \Delta\lambda_2 \end{bmatrix} \tag{9}$$

The relationship among the liquid level and temperature and wavelength drifts can be obtained by substituting the measured experimental sensitivities into the matrix formula:

$$\begin{bmatrix} \Delta L \\ \Delta T \end{bmatrix} = \frac{1}{13.426} \begin{bmatrix} -0.346 & 0.327 \\ -343.71 & 363.64 \end{bmatrix} \begin{bmatrix} \Delta\lambda_1 \\ \Delta\lambda_2 \end{bmatrix} \tag{10}$$

Eq. (10) can be used for measuring the liquid level and temperature. Besides, the proposed sensor can realize multi-parameter detection of liquid level, temperature, and RI.

Fig. 10 shows the stability of the proposed sensor based on M-ORCP. Fig. 10(a) is the reflection spectra measured for 1 *h*. The insets are the details of the wavelength dips around 1532 nm and 1557 nm and Fig. 10(b) shows the measured wavelength fluctuations. The wavelength shifts are all $< \pm 0.01$ nm, indicating the proposed sensor has high stability.

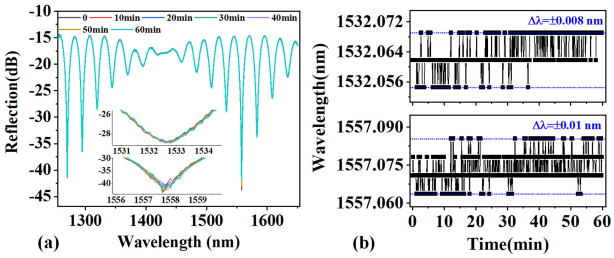

Fig. 10. Measured stability of the OFLLS for 60 min: (a) The reflection spectra; (b) The wavelength fluctuations around 1532 nm and 1557 nm.

V. Conclusion

In conclusion, we demonstrate multi-parameter sensors based on ORCP, for detection of liquid level, temperature, and RI. The liquid level sensitivities of S-ORCP, F-ORCP and M-ORCP are 43.71 nm/mm, 65.14 nm/mm, and 363.64 nm/mm around 1550 nm, respectively. The highest liquid level sensitivity is achieved by the M-ORCP and the detection limit is as low as 0.06 μm. The temperature and RI can also be detected by the M-ORCP, with sensitivities of -0.327 nm/°C and 7859.27 nm/RIU, respectively. The proposed ORCP sensors of $\sim$ cm length can measure the liquid level range of $\sim$3 mm due to the merits of high sensitivity, stability, and compact half-coupler probe structure, which have broad application prospects in the fields of fuel storage and chemical liquid level measurement, especially for chemical reagents, biological tissue liquids and flammable and explosive liquids.

References

[1] K. Yamada, S. Horiuchi, H. Honda, and T. Kinai, "A novel approach in liquid-level sensing by trapped-energy-mode thickness vibrators," in *Proc. IEEE Int. Ultrasonics Symp.*, 2009, pp. 2508–2510.

[2] C. A. Gong, H. K. Chiu, L. R. Huang, C. H. Lin, Z. D. Hsu, and P.-H. Tu, "Low-cost comb-electrode capacitive sensing device for liquid-level measurement," *IEEE Sensors J.*, vol. 16, no. 9, pp. 2896–2897, May 2016.

[3] Y. Liu, Y. Li, X. Yan, and W. Li, "High refractive index liquid level measurement via coreless multimode fiber," *IEEE Photon. Technol. Lett.*, vol. 27, no. 20, pp. 2111–2114, Oct. 2015.

[4] W. Liu, X. Wu, and G. Zhang, "Thin fiber-based Mach-Zehnder interferometric sensor for measurement of liquid level, refractive index, temperature, and axial strain," *Appl. Opt.*, vol. 59, no. 6, pp. 1786–1792, Feb. 2020.

[5] D. Liu et al., "Sub-micrometer resolution liquid level sensor based on a hollow core fiber structure," *Opt. Lett.*, vol. 44, no. 8, pp. 2125–2128, Apr. 2019.

[6] J. Kang, L. Hou, Z. Li, X. Liu, X. Zhang, and J. Yang, "Low refractive-index and temperature crosstalk fiber-optic liquid level sensor based on cascaded quasi-microfiber and double-cladding fiber structure," *IEEE Sensors J.*, vol. 21, no. 2, pp. 1554–1560, Jan. 2021.

[7] J. E. Antonio, J. J. Sanchez, and P. Likamwa, "Fiber-optic sensor for liquid level measurement," *Opt. Lett.*, vol. 36, no. 17, pp. 3425–3427, Sep. 2011.

[8] Y. Wang, G. Yan, and Z. Lian, "Liquid-level sensing based on a hollow core Bragg fiber," *Opt. Exp.*, vol. 26, no. 17, pp. 21656–21663, Aug. 2018.

[9] M. Zhang et al., "Power-type liquid level sensor for high refractive index liquid based on long-period fiber grating," *Sensors Actuators A: Phys.*, vol. 324, Jun. 2021, Art. no. 112652.

[10] C. A. R. Diaz et al., "Liquid level measurement based on FBG-embedded diaphragms with temperature compensation," *IEEE Sensors J.*, vol. 18, no. 1, pp. 193–200, Jan. 2018.

[11] Y. Dong, S. Xiao, H. Xiao, J. Liu, C. Sun, and S. Jian, "An optical liquid level sensor based on D-shape fiber modal interferometer," *IEEE Photon. Technol. Lett.*, vol. 29, no. 13, pp. 1067–1070, Jul. 2017.

[12] R. Fan et al., "Liquid level and refractive index double-parameter sensor based on tapered photonic crystal fiber," *J. Lightw. Technol.*, vol. 38, no. 14, pp. 3717–3722, Jul. 2020.

[13] J. Wang et al., "Highly sensitive liquid-level sensor based on an optical reflective microfiber probe," *Opt. Lett.*, vol. 45, no. 1, pp. 2125–2128, Jan. 2020.

[14] Y. Zhang et al., "High sensitivity optical fiber liquid level sensor based on a compact MMF-HCF-FBG structure," *Meas. Sci. Technol.*, vol. 29, no. 5, pp. 055104–055110, May 2018.

[15] L. Bao, X. Dong, P. Shum, and C. Shen, "High sensitivity liquid level sensor based on a hollow core fiber structure," *Opt. Commun.*, vol. 499, no. 15, 2021, Art. no. 127279.

[16] L. Liang, L. Jin, Y. Ran, L. P. Sun, and B. O. Guan, "Interferometric detection of microRNAs using a capillary optofluidic sensor," *Sensors Actuators B: Chem.*, vol. 242, pp. 999–1006, Apr. 2017.

[17] K. Li, N. Zhang, and L. Wei, "Birefringence induced Vernier effect in optical fiber modal interferometers for enhanced sensing," *Sensors Actuators B: Chem.*, vol. 275, pp. 16–24, Dec. 2018.

[18] K. Li, M. Zhang, and Z. Nan, "Spectral characteristics and ultrahigh sensitivities near the dispersion turning point of optical microfiber couplers," *J. Lightw. Technol.*, vol. 36, no. 12, pp. 2409–2415, Jun. 2018.

[19] J. J. Wang, X. Li, J. Fu, and K. Li, "High-sensitivity, large dynamic range refractive index measurement using an optical microfiber coupler," *Sensors*, vol. 19, no. 23, Dec. 2019, Art. no. 5078.

[20] G. Pelegrina et al., "Analysis of the modal evolution in fused-type mode-selective fiber couplers," *Opt. Exp.*, vol. 23, no. 18, pp. 22977–22990, Sep. 2015.

[21] K. Ogawa, "Simplified theory of the multimode fiber coupler," *Bell Syst. Tech. J.*, vol. 56, no. 5, pp. 729–745, Jun. 1977.

[22] M. Ding, P. Wang, and G. Brambilla, "A microfiber coupler tip thermometer," *Opt. Exp.*, vol. 20, no. 5, pp. 5402–5408, Feb. 2012.

[23] M. Xiong, H. Gong, Z. Qian, C. L. Zhao, and X. Dong, "Simultaneous measurement of liquid level and temperature based on spherical-shape structures and long period fiber grating," *Sensors Actuators, A Phys.*, vol. 239, pp. 196–200, Mar. 2016.

[24] M. Song, Y. Zhang, and J. He, "Measuring the relationship between liquid refractive index and temperature with Michelson interferometer," *J. Qinghai Univ.*, vol. 33, no. 15, Oct. 2015, Art. no. 5.